Digest Journal of Nanomaterials and Biostructures Vol. 6, No 1, January-March 2011, p. 169 - 179

PREPARATION OF SIZE CONTROLLED, STOICHIOMETRIC AND BIORESORBABLE HYDROXYAPATITE NANOROD BY VARYING INITIAL pH, Ca/P RATIO AND SINTERING TEMPERATURE

M. RAJKUMAR, N. MEENAKSHI SUNDARAM, V. RAJENDRAN*
Centre for Nanoscience and Technology, K.S. Rangasamy College of Technology Tiruchengode-637 215, Tamil Nadu, India

To control the particle size, morphology and stoichiometry of hydroxyapatite (HAp) is very important in properties and applications. HAp plays a keyrole in the field of orthopedic and dental because of it's appreciable host responses in the biological environment. The aqueous based sol-gel method has been employed to synthesis a size controlled HAp with nanorod like morphology. It has been found that the variation in molar concentration of initial sols and pH can be used to control the Ca/P ratio of the final product, crystallite size and surface morphology of the HAp. The stoichiometric (Ca/P=1.67) HAp nanorod (48-52 nm x 15-18 nm) has been achieved against initial molar concentration ratio of 1.72 and pH=11. Further, the optimised stoichiometric HAp nanorod is sintered at three different temperatures to investigate the effect of sintering temperature on morphology, microhardness and bioresorbability. The nanorod like morphology in the powder changed to a more equiaxed shape (spherical like morphology with size of 85.24 nm) after sintering. The crystallite size of HAp nanorod is increases with increase the pH and Ca/P ratio. Further, it has been observed that the hardness of the HAp nanorod increases with increase in the sintering temperature.

(Received Deccamber 3, 2010; accepted January 15, 2011)

Keywords: Hydroxyapatite nanorod, Sol-gel, Bioresorbability, Microhardness

1. Introduction

A material that elicits a specific biological response at the interface of the material, which results in the formation of a bond between the tissue and the material is known as bioactive material. Hydroxyapatite (HAp) is a class of calcium phosphate containing water in the chemical composition as $Ca_{10}(PO_4)_6(OH)_2$ with a Ca/P molar ratio is 1.67. HAp is the least degradable form among various calcium phosphates, insoluble in neutral and alkaline solutions [1]. HAp is a major mineral component present in the calcified tissues like bone and teeth. The importance of HAp has led to an extensive research in numerous areas ranging from the biomedical to industrial applications. Synthetic HAp has an excellent biocompatibility and bioactivity which leads to numerous potential applications like reconstruction of damaged bone or tooth zones [2], matrices for controlled drug release [3], bone cements [4], tooth paste additives [5], bone tissue engineering [6] etc. In addition to the biomedical applications, HAp finds wide application in other areas such as a catalyst in chromatography or gas sensor, water purification and fertilizers production [7]. Generally, HAp is used in the form of densified powders or paste or polymer composites in load bearing orthopedic and dental applications [2].

However, it is difficult to obtain the exact stoichiometry (Ca/P ratio) in HAp because of different Ca/P ratios which can be stabilized depends on the synthesis method and conditions employed. Various HAp phases such as calcium-deficient HAp, oxy-HAp and carbonate-substituted HAp depends on the type of environment employed during the synthesis steps [8]. A

*Corresponding author: veerajendran@gmail.com

number of processing routes have been developed for synthesizing the nano HAp such as co-precipitation, hydrothermal, sol-gel, solid-state reaction and so on [9]. Among the alternative methods, sol-gel synthesis of HAp powders has been recently attracted much attention due to their many advantages, which include high product purity, homogeneous molecular mixing and low processing temperature [10]. The sol-gel process method requires a strict pH control, vigorous agitation and takes long time for hydrolysis. The sol–gel synthesis of pure HAp powder has been extensively revealed to tune the properties of HAp, including bioactivity, biocompatibility, solubility, sinterability, castability, fracture toughness and absorption.

The optimisation of the compositions of the calcium and phosphate precursors is essentially required to obtain the HAp final product with a stoichiometric ratio of 1.67. Thus, the tailoring the required properties of HAp can be made over a wide range by controlling the composition, particle size and morphology. In order to meet the requirements, it is of great importance to develop HAp synthesis methods focused on the precise control of particle size, morphology and chemical compositions.

In the present work, an inexpensive precursor has been used to obtain the nano-rod like morphology of HAp powder by water based sol-gel method without using any surfactant. The role of molar concentration of initial solution and pH value on the particle size, morphology and composition of HAp have been investigated. Further, to study the sintering effect on morphology, hardness and bioresorbability of optimised stoichiometric HAp nanorod.

2. Materials and methods

2.1. Materials

HAp with nanorod like morphology was prepared by simple aqueous based sol-gel method from the precursor of calcium nitrate tetrahydrate ($Ca(NO_3)_2.4H_2O$) and di-ammonium hydrogen phosphate ($(NH_4)_2HPO_4$). The starting materials used were of Analytical grade (AR) high pure calcium nitrate tetrahydrate (Merck, 99.9%), di-ammonium hydrogen phosphate (Merck, 99.9%), ammonia solution (Merck, min. 25% Guaranted reagent (GR)) and ultra pure water (Sartorius (AG), Arium 611Ultra filter (UF), Germany).

2.2. Synthesis of nano HAp

The HAp nanorod powders were obtained from the precursors of different molar concentrations ratio i.e., 1.72, 1.67 and 1.53 with pH value of 10 (hereafter called as HAp-A1, HAp-B1 and HAp-C1 respectively). The pH value of the prepared solutions were increased from 10 to 11 by adding the ammonium hydroxide, in all the molar concentrations i.e., 1.72, 1.67 and 1.53 (hereafter called as HAp-A2, HAp-B2 and HAp-C2 respectively) as shown in Table 1. The different concentrations with pH 10 and 11 of the solution were prepared employing the following procedure. The required molar concentrations of the initial precursors were dissolved in a ultrapure water (pH 7.2 ± 0.19) separately and then, the solution was stirred until the starting material is completely dissolved. The pH value of both calcium and phosphate solution was adjusted separately to 10 and 11 using ammonia hydroxide. A drop wise addition (1 ml/min) of phosphate containing solution was added to the calcium containing solution under vigorous stirring. Then, the mixed solution was thoroughly stirred for 1 h. The mixed solution is kept at 80 ºC for 24 h to obtain the gel. Then, the gel was dried at 80 ºC to obtain the hydroxyapatite powder. A similar procedure was employed to prepare the different molar concentrations. In addition to that the optimised stoichiometric hydroxyapatite nanorod (HAp-A2) was sintered at three different temperatures such as 300, 600 and 900 ºC (hereafter sintered samples were assigned as HAp-A2-300, HAp-A2-600 and HAp-A2-900).

Table 1 Experimental conditions and values of crystallite size, lattice parameters and unit cell volume of Hap.

S. No	Sample name	Ca^{2+}	PO_4^{3-}	Initial Ca/P ratio	pH	Crystallite size	Lattice Parameters		Unit cell volume
		g mol^{-1}	g mol^{-1}			nm	a Å	c Å	$Å^3$
1.	HAp-A1	1	0.58	1.72	10	5.3720	9.3720	6.9039	525.1655
2.	HAp-A2	1	0.58	1.72	11	7.3013	9.4131	6.8791	527.8838
3.	HAp-B1	1	0.60	1.67	10	11.4640	9.4168	6.8878	528.9638
4.	HAp-B2	1	0.60	1.67	11	17.1511	9.4029	6.8790	526.7231
5.	HAp-C1	1	0.65	1.53	10	14.7727	9.4203	6.8913	529.6264
6.	HAp-C2	1	0.65	1.53	11	22.6210	9.4584	6.8914	533.9319
7.	HAp-A2-300	1	0.58	1.72	11	8.4121	9.4261	6.8951	530.5703
8.	HAp-A2-600	1	0.58	1.72	11	11.4716	9.4373	6.9065	532.7108
9.	HAp-A2-900	1	0.58	1.72	11	57.7282	9.4102	6.8721	527.0215

2.3. Structural and morphological characterisation

The obtained nano powders were characterised by the following techniques: the phase identification was performed by X-ray (XRD, X' Pert Pro, PANalytical, Netherland) diffractometer using CuK_{α}, (λ=1.5406 Å) as a radiation source over the 2θ range of 10 - 80º at 25º C. The Fourier transform infrared spectroscopy (FTIR, PerkinElmer, Spectrum 100, USA) was used in the wave number region of 4000 –400 cm^{-1} to obtain the characteristic peaks of HAp powders. The composition and morphology of all the samples have been examined employing respectively the energy dispersive X-Ray analysis (EDAX) and scanning electron microscopy (SEM, Jeol, Jsm 6360, Japan) and transmission electron microscopy (TEM, Philips, CM 200, USA) studies.

2.4. *In vitro* bioresorbability test

In vitro bioresorbability testing of the sintered samples were conducted by immersing the samples in simulated body fluid (SBF) of pH 7.4. The SBF solution was prepared using 9 g NaCl, 5 g KCl and 0.2 g $MgHPO_4.3H_2O$/L [11]. Each sample (1mg/ml) was immersed in 50 ml SBF solution which was kept in a polyethylene bottle covered with a tight lid in a water bath at 37 °C. The bottles were placed in a constant temperature bath maintained at 37 ºC for two weeks. The pH of SBF was measured every day during the soaking periods of 0 to 14 days.

2.5. Vickers microhardness test

The Vickers microhardness measurements for as-synthesised (HAp-A2-0) and sintered (HAp-A2-300, HAp-A2-600 and HAp-A2-900) samples of HAp nanorod have been performed on Bareiss microhardness tester (Bareiss, Germany). The samples are uniaxially compressed in a stainless steel pellet die for 4 min at a pressure of 100 kg cm^{-2} to make a circular disc as in the size of 13 mm diameter and 2-3 mm thickness. Five indentations were made for each sample and the average value was taken.

3. Results and discussion

3.1. SEM/EDAX studies

The EDAX and SEM pattern of HAp-A1, HAp-A2, HAp-B1 and HAp-B2, HAp-C1, HAp-C2 samples are given in Fig 1. The EDAX results confirmed the existence of the elements such as Ca, P and O. From the EDAX pattern, it can be seen that the Ca/P ratio oscillates between 1.26 and 1.56, which indicates the formed HAp is calcium deficient HAp. Fig. 1b reveals that the formed HAp with Ca/P= 1.67 against the initial molar concentration ratio of 1.72 and pH = 11 of the solution. The Ca/P ratio of the prepared samples increases with increase in the pH value. The SEM study exhibits the formation of HAp with dense surface morphology. This is possibly due to the recrystallization of the dissolved calcium nitrate during the gel formation and the subsequent drying processes. The same can be removed by proper sintering process [12]. Thus, it indicates that the final Ca/P ratio depends on both the initial concentration and the pH value.

3.2. X-ray diffraction (XRD) analysis

The phase analysis is performed from the recorded X-ray diffraction patterns of HAp-A1 & HAp-A2, HAp-B1 & HAp-B2 and HAp-C1 & HAp-C2 samples as shown in Fig. 2. From the XRD patterns, diffraction peaks have been identified as hexagonal phase of HAp powder (JCPDS card no. 09-0432). The observed sharp peaks in the XRD patterns in all the samples confirm that the samples are in the crystalline nature. The crystallite size of HAp is determined using the Scherrer formula [13],

$$D = \frac{0.9\lambda}{\beta Cos\theta} \tag{1}$$

where D is the crystallite size calculated for the (h k l) reflection, λ the wavelength of CuK_{α} radiation (1.5406 Å), β the full width of the peak at half of the maximum intensity (FWHM) and θ the diffraction angle of the corresponding reflection. The estimated crystallite size and lattice parameters values are shown in Table 1.

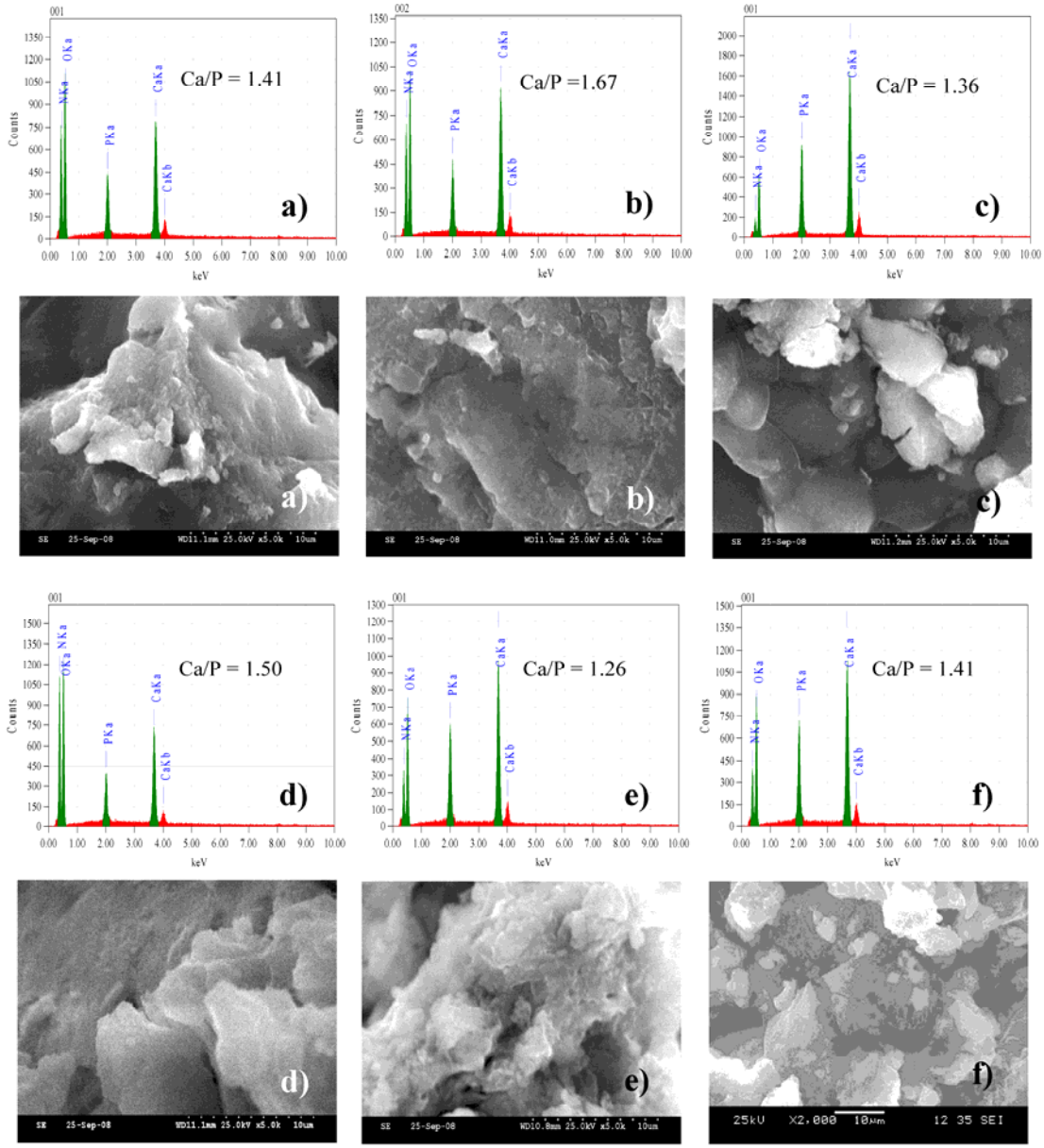

Fig. 1. SEM/EDAX pattern of a) HAp-A1, b) HAp-A2, c) HAp-B1, d) HAp-B2, e) HAp-C1, f) HAp-C2.

The observed results (Table 1) indicate that an increase in the pH value and molar concentration with increase in the crystallite size. The lattice parameters are calculated based on the relationship between lattice spacing (d) and lattice parameters (a, c) of the hexagonal structure, expressed as,

$$\frac{1}{d^2} = \frac{4}{3}\left(\frac{h^2 + hk + k^2}{a^2}\right) + \frac{l^2}{c^2} \tag{2}$$

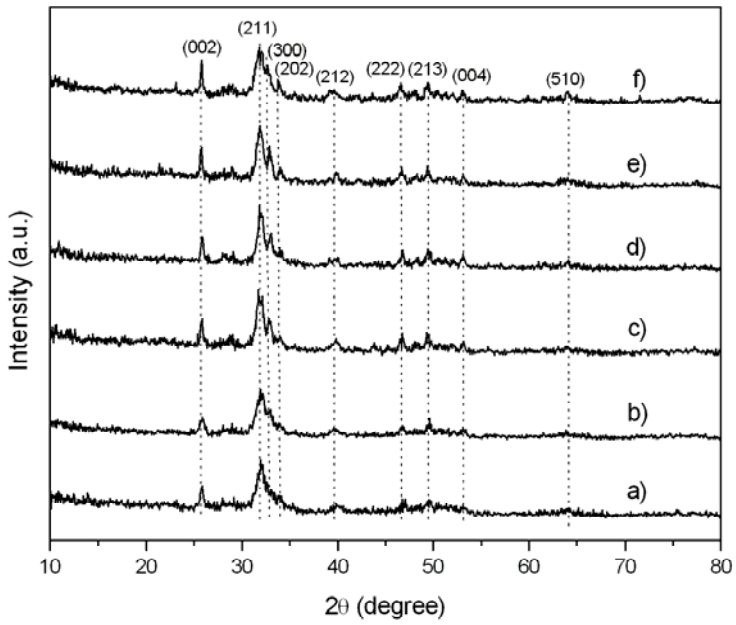

Fig. 2. XRD Pattern of a) HAp-A1, b) HAp-A2, c) HAp-B1, d) HAp-B2, e) HAp-C1, f) HAp-C2

where d is the crystallite size, h, k & l are Miller indices of the plane and a & c are lattice constant. The standard lattice constants a = 9.418 Å and c = 6.884 Å (JCPDS card no. 09-0432) for the HAp has been matched well with the obtained values in the present study. Fig. 3 shows that XRD pattern of sintered stoichiometric HAp nanorod i.e., HAp-A2, HAp-A2-300, HAp-A2-600 and HAp-A2-900.

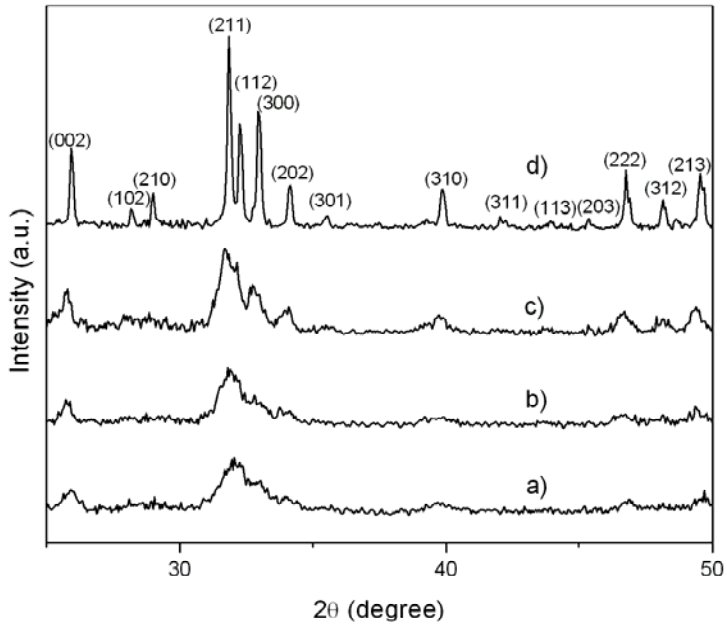

Fig. 3. XRD pattern of a) HAp-A2, b) HAp-A2-300, c) HAp-A2-600, d) HAp-A2-900

The intensity of the peaks reflects that the samples are highly nanocrystalline nature. It can be seen that crystallinity and crystallite size increases with increasing the sintering temperature.

3.3. Fourier transform infrared spectroscopy (FTIR) analysis

The Fourier transform infrared spectra of sintered stoichiometric HAp nanorod are shown in Fig. 4.

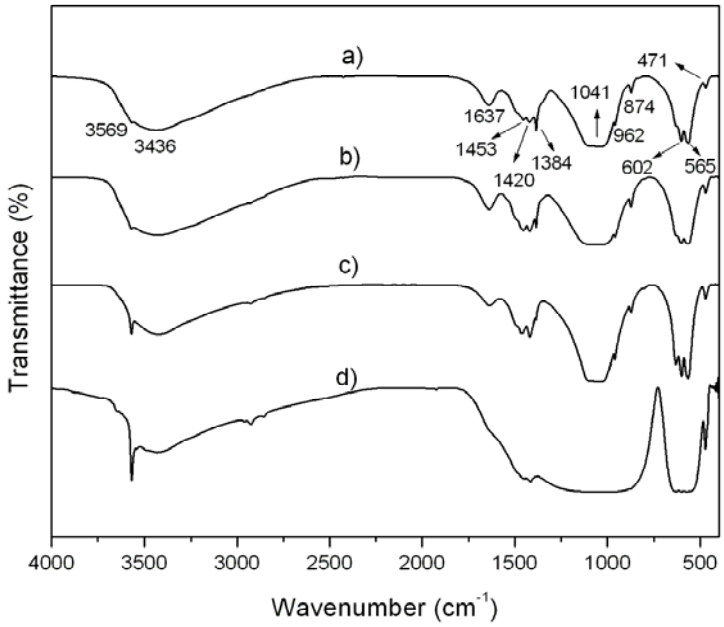

Fig. 4. FTIR spectra of a) HAp-A2, b) HAp-A2-300, c) HAp-A2-600, d) HAp-A2-900

The characteristic peaks are listed in Table 2. The bands appeared at 962 and 471 cm^{-1} indicates the symmetric stretching modes (ν_1 and ν_2) of phosphate group respectively [14].

Table 2 Characteristic infrared bands of HAp compounds.

S.No.	Vibrational frequency cm^{-1}	Assignments
1.	962 and 471	Symmetric stretching modes (ν_1 and ν_2) of phosphate group [14]
2.	566 and 603	O-P-O bending bands [15]
3.	3569-3571 and 631-635	Stretching vibration of the HAp hydroxyl group [16]
4.	1041-1091	ν_3 P-O asymmetric stretching [17]
5.	874, 1380-1466	Atmosphere carbon dioxide [18,19]
6.	3430-3431 and 1634-1637	Presence of lattice water [20]

Further, the O-P-O bending bands have been observed at 566 and 603 cm^{-1} due to presence of nano HAp [15]. The bands at 3569-3571 cm^{-1} and 631-635 cm^{-1} due to stretching vibration of the HAp hydroxyl group. This may be originating from libration bands of OH group [16]. The ν_3 P-O asymmetric stretching appeared in the region of 1041-1091 cm^{-1} [17]. The presence of carbonate ions in the synthesised HAp particles have been assigned at 874, 1380-1466 cm^{-1}, which may comes from the atmosphere carbon dioxide during the synthesis [18,19]. The bands at 3430-3431 cm^{-1} and 1634-1637 cm^{-1} in HAp are owing to the presence of lattice water in the solid [20].

Thus, the drastic decrease in the content of water with an increase the sintering temperature. According to the FTIR result, there is no marked evidence for any other impurities.

3.4. Transmission electron microscopy (TEM) analysis

The particle size and morphology of the sintered stoichiometric HAp nanorod have been further examined by TEM. Fig.5 reveals the TEM photographs of the samples HAp-A2, HAp-A2-300, HAp-A2-600 and HAp-A2-900.

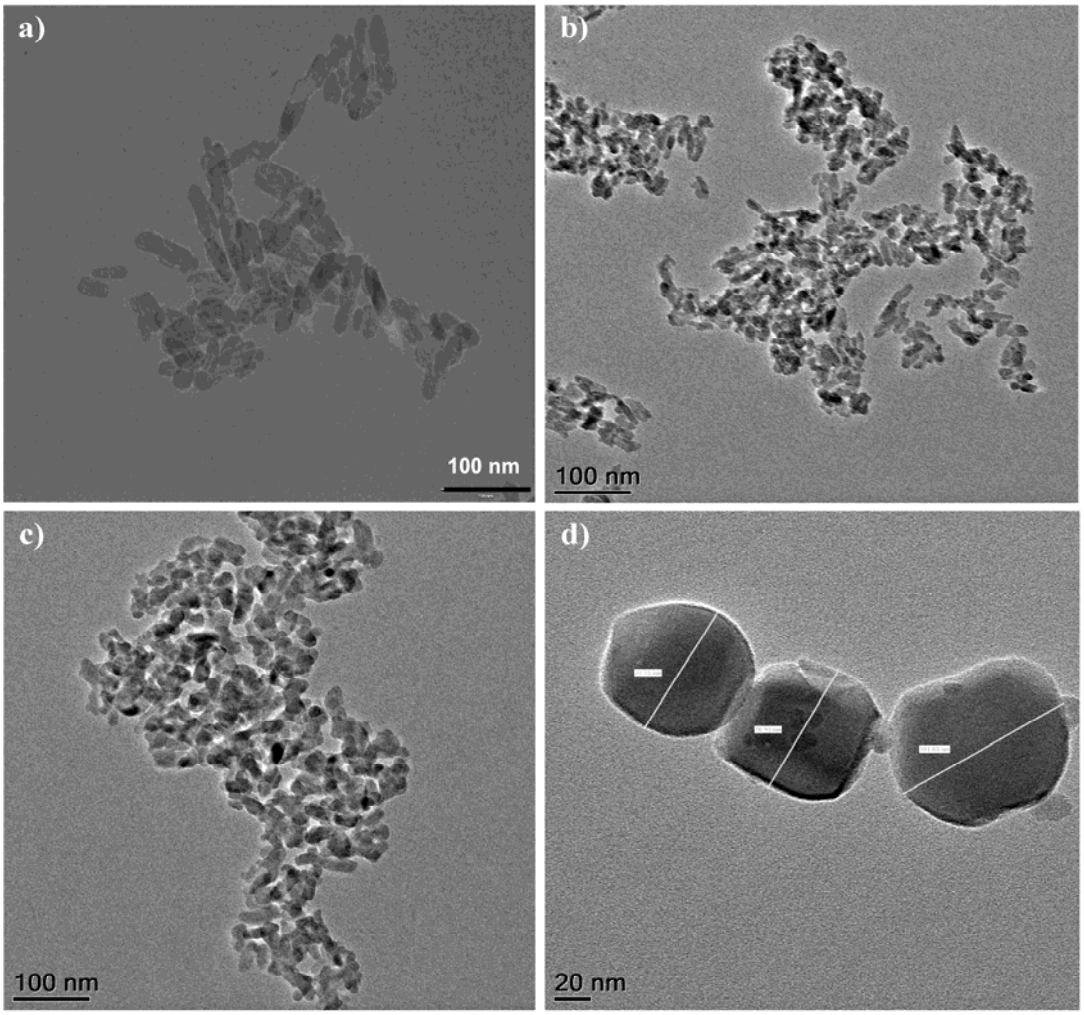

Fig. 5. TEM micrograph of a) HAp-A2, b) HAp-A2-300, c) HAp-A2-600, d) HAp-A2-900.

The samples exhibit relatively uniform distribution with nanorod like morphology as shown in Fig 5a. The average length and width of (HAp-A2) the nanorod like morphology is 48-52 nm and 15-18 nm. The nanorod morphology is linearly become a spherical morphology (average particle size is 85.24 nm) when increase the sintering temperature to 900 °C.

3.5. *In vitro* bio-resorbability test

Fig. 6 shows that the graph of pH variation with soaking period in SBF medium for sintered samples of HAp-A2, HAp-A2-300, HAp-A2-600 and HAp-A2-900. The pH decreases with increasing the soaking period has observed for HAp-A2 and HAp-A2-300 samples. In case of HAp-A2-600 and HAp-A2-900 samples, pH is suddenly increases with increasing the soaking

period initially and then decreases with further increasing the soaking periods. The initial pH variations in the alkaline region may be due to release of PO_4^{3-} than Ca^{2+} ions. The pH value is depend on solubility or resorbability of the HAp with soaking period in body fluid i.e., the pH decreases as the solubility increases [21].

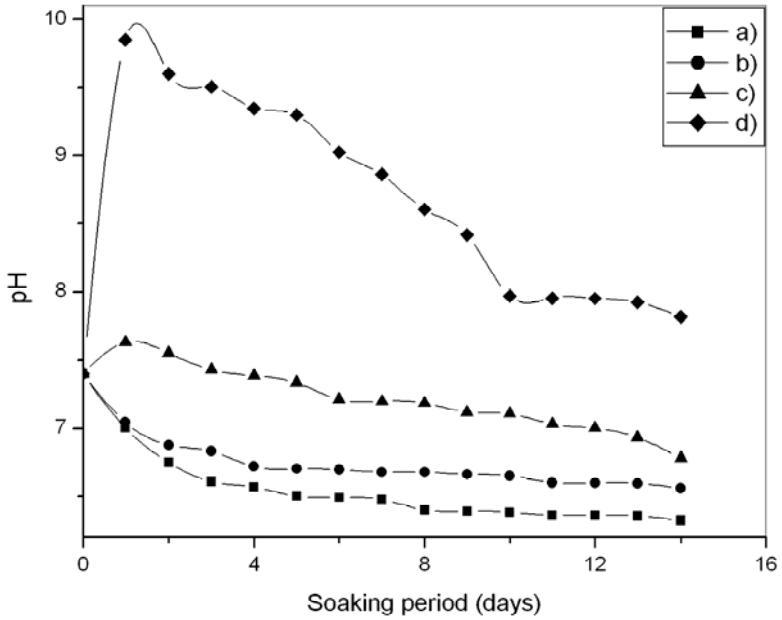

Fig. 6. In vitro bioresorbability of a) HAp-A2, b) HAp-A2-300, c) HAp-A2-600, d) HAp-A2-900 as a function of soaking period

Based on the graph, it is clear that there are notable evidences for resorbability for all samples. Further it can be seen that resorbability varies with respect to sintering temperature of the sample. The sintering temperature increases (particle size increases) with decreasing the resorbability. According to this result, the resorbability can be altered by controlling the particle size.

3.6. Vickers microhardness test

Vickers microhardness of sintered samples is shown in Fig. 7. The hardness of HAp increases with increase the sintering temperature. The calculated density also increases with sintering temperature. During the sintering, the particles are closely packed to form as a dense material. Also, this densification may be the reason to increases the hardness as well as particles size with sintering temperature. This hardness study has further support the observation made in TEM studies. The maximum hardness of 52.15 HV has been observed at 900 ºC. It has been found that sintering temperature gives significant effect on the hardness.

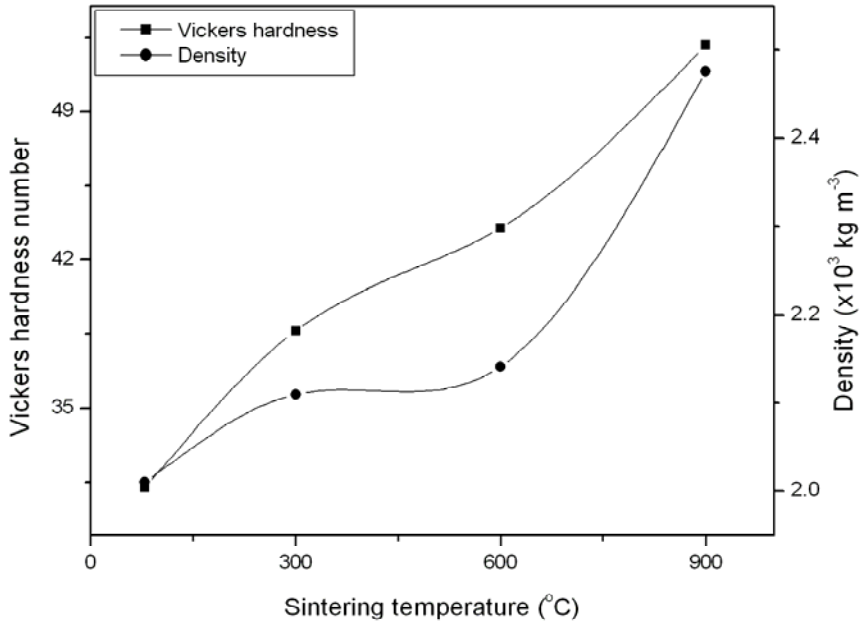

Fig. 7. Variations of microhardness and density as a function of sintering temperature

4. Conclusion

In the present investigation, the pure nanorod like HAp was synthesised employing aqueous based sol-gel method without using any surfactant. The EDAX studies confirm the Ca/P ratio depends on both initial molar concentration and pH values. The hexagonal structure of the prepared nano HAp has been confirmed from the XRD results. The average crystallite size of the HAp is in the range between 5 to 57 nm. As the molar concentration ratio increases, the crystallite size gets reduced. Also as pH increases with the crystallite size gets increased from XRD measurements. It was noticed that the pH value has a significant effect on the crystallite size. The TEM result suggests that the stoichiometric HAp exhibit particle with nanorod like morphology. The nanorod morphology slowly becomes to as spherical like (equiaxed shape) morphology with increases the sintering temperature. The bioresorbability of HAp can be altered by controlling the particle size and sintering temperature. It is believed that the process developed in the present work is also applicable for the preparation of hydroxyapatite-based solid state solutions to obtain a size controlled and bioresorbable nano HAp. The obtained HAp nano powder can be used for various biomedical applications.

Acknowledgement

The authors are thankful to the Department of Science and Technology (DST), New Delhi for the financial support to carry out this research project (SR/S2/CMP-66/2006 dt.27.09.2007). We would like to acknowledge Dr.A.Rajadurai and Dr.K.Kalaichelvan, Department of Production Technology, Madras Institute of Technology, Chennai in extending facilities to do microhardness measurement.

References

[1] C. P. A. T. Klein, J. M. A. D. Blieck-Hogemrst, J. G. C. Wolket, K. De Groot, Biomaterials **11**, 509 (1990).
[2] S. V. Dorozhkin and M. Epple, Angew. Chem. Int. Ed., **41**, 3130 (2002).
[3] R. Z. Legeros, Adv. Dent. Res., **2**, 164 (1998).

[4] M. Itokazu, W. Yang, T. Aoki, A. Ohara, N. Kato, Biomaterials **19**, 817 (1998).
[5] S. M. Kenny and M. Buggy, J. Mater. Sci. Mater. Med., **14**, 923 (2003).
[6] D. A. Wahl, E. Sachlos, C. Liu and J. T. Czernuszka, J. Mater. Sci. Mater. Med., **18**, 201 (2007).
[7] J. Torrent-Burgues and R. Rodriguez-Clemente, Cryst. Res. Technol., **36**, 1075 (2001).
[8] D. Choi and P. N. Kumta, J. Am. Ceram. Soc., **89**, 444 (2006).
[9] W. Suchanek and M. Yoshimura, J. Mater. Res., **13**, 94 (1998).
[10] D. M. Liu, T. Troczynski and W. J. Tseng, Biomaterials **22**, 1721 (2001).
[11] F. C. M. Driessens, M. G. Boltong, E. A. P. De Maeyer, R. Wenz, R. Nies, J. A. Planell, Biomaterials **23**, 4011 (2002).
[12] Il-Seok Kim and P. N. Kumta, Mater. Sci. and Eng. B **111**, 232 (2004).
[13] E. Bouyer, F. Gitzhofer and M. I. Boulos, J. Mater. Sci. Mater. Med., **11**, 523 (2000).
[14] S. H. Rhee, J. Mater. Sci. Mater. Med., **13**, 597 (2002).
[15] V. Thomas, D. R. Dean, M. V. Jose, B. Mathew, S. Chowdhury, Y. K. Vohra, Biomacromolecules **8**, 631 (2007).
[16] Y. Zhang and J. Lu, Cryst. Growth. Des., **8**, 2101 (2008).
[17] A. Lak, M. Mazloumi, M. Mohajerani, A. Kajbafvala, S. Zanganeh, H. Arami, S. K. Sadrnezhaad, J. Am. Ceram. Soc., **91**, 3292 (2008).
[18] D. Z. Chen, C. Y. Tang, K. C. Chan, C. P. Tsui, P. H. F. Yu, M. C. P. Leung and P. S. Uskokovic, Compos. Sci. Technol., **67**, 1617 (2007).
[19] W. Zhang, S. S. Liao and F. Z. Cui, Chem. Mater., **15**, 3221 (2003).
[20] C. C. Ribeiro, I. Gibson and M. A. Barbosa, Biomaterials **27**, 1749 (2006).
[21] R. Murugan and S. Ramakrishna, J. Cryst. Growth **274**, 209 (2005).